Chemical Geology 545 (2020) 119639

Contents lists available at ScienceDirect

Chemical Geology

journal homepage: www.elsevier.com/locate/chemgeo

Unusually homogeneous helium isotope composition of the Auckland Volcanic Field and its implications for the underlying mantle

Michael C. Rowe[a,*], David W. Graham[b], Elaine Smid[a], Lucy McGee[c]

[a] School of Environment, University of Auckland, Auckland 1142, New Zealand
[b] College of Earth, Ocean, and Atmospheric Sciences, Oregon State University, Corvallis, OR 97331, USA
[c] Department of Earth Sciences, School of Physical Sciences, University of Adelaide, Adelaide, Australia

ARTICLE INFO

Editor: Don Porcelli

Keywords:
Mantle heterogeneity
Helium isotopes
Trace elements
Zealandia
Volatiles
Degassing

ABSTRACT

The Auckland Volcanic Field (AVF) is one of the most intensively studied monogenetic basalt fields in the world yet its origin remains enigmatic. Magmatism in the AVF occurred from ~193 ka to 500 years bp. The trace element and isotopic diversity of AVF basalts require "small-scale" compositional heterogeneity in the underlying mantle that is comparable in volume to, or slightly larger than, the scale of individual eruptions in the AVF.

Olivine from tephra and lava, representing the range of AVF compositions, was crushed and analysed for $^3He/^4He$, and He and CO_2 concentrations in an attempt to further characterize and explain the significance of the AVF "end-members". AVF basalts show a negative covariation between the amount of CO_2 released by crushing of olivine and the whole rock concentrations of highly incompatible trace elements, such as Ba, Rb, Nb, Zr, Ti and K. In contrast, the amount of He released by crushing shows no simple relations with the same incompatible elements or their ratios. This leads to a significant variation in $CO_2/^3He$ ratios (9.4×10^7–3.5×10^9) that may relate to differences in magma ascent dynamics, as well as to different magma sources. The measured CO_2/He ratios may have been influenced by varying amounts of CO_2 diffusion into vapour bubbles within melt inclusions that depend on melt composition and magma ascent rate. However, petrographically there is no evidence for systematic differences in the size or quantity of vapour bubbles in olivine-hosted melt inclusions.

$^3He/^4He$ ratios in 14 AVF samples studied here show a narrow range from 6.57 to 7.26 R_A (mean of 7.10 ± 0.26). This may imply a dominance of the mantle helium budget by small-scale heterogeneities. Alternatively, the $^3He/^4He$ results suggest that the tectonic and magmatic history of the mantle beneath the AVF has effectively hybridized the $^3He/^4He$ ratio to a larger extent than for highly incompatible trace element ratios and Pb-Nd-Sr isotopes. The value of ~7 R_A for the mantle source of AVF basalts, in light of other evidence, suggests that there is a relatively homogeneous He isotope composition for the Zealandia-Antarctic mantle domain.

1. Introduction

Monogenetic basaltic volcanic fields can show a wide range of compositional diversity (Strong and Wolff, 2003; Haase and Renno, 2008; Nichols et al., 2012; McGee et al., 2013; Rasoazanamparany et al., 2015; Hopkins et al., 2016). The relatively small volume (< 0.1 km^3), and implied lower degree partial melts associated with monogenetic eruptions, provide an opportunity to investigate mantle processes and materials lost to homogenization in larger magmatic systems (e.g. Stracke and Bourdon, 2009; McGee and Smith, 2016). The geochemical heterogeneity is often ascribed to a multitude of magmatic processes from the mantle through the crust, such as crystal fractionation (Johnson et al., 2008) and melt transport/extraction effects that include melt/wallrock reequilibration or magma mixing (Reiners, 1998; Stracke and Bourdon, 2009). However, the chemical diversity and the presence of multiple geochemical components, observed both during and between discrete eruptions in a monogenetic field (based on variations in major and trace element abundances and isotopic ratios) is often beyond what can be reasonably explained by melting of a homogeneous mantle source (Strong and Wolff, 2003). This isotopic and trace element heterogeneity of monogenetic basalts is often cited as evidence for the melting of localized mantle heterogeneities (e.g. McGee et al., 2013; Rasoazanamparany et al., 2015; McGee and Smith, 2016).

The Auckland Volcanic Field (AVF; Fig. 1), located within the populated city centre of Auckland, New Zealand (population 1.6 million at

* Corresponding author.
E-mail address: Michael.rowe@auckland.ac.nz (M.C. Rowe).

https://doi.org/10.1016/j.chemgeo.2020.119639
Received 9 December 2019; Received in revised form 12 April 2020; Accepted 16 April 2020
Available online 26 April 2020

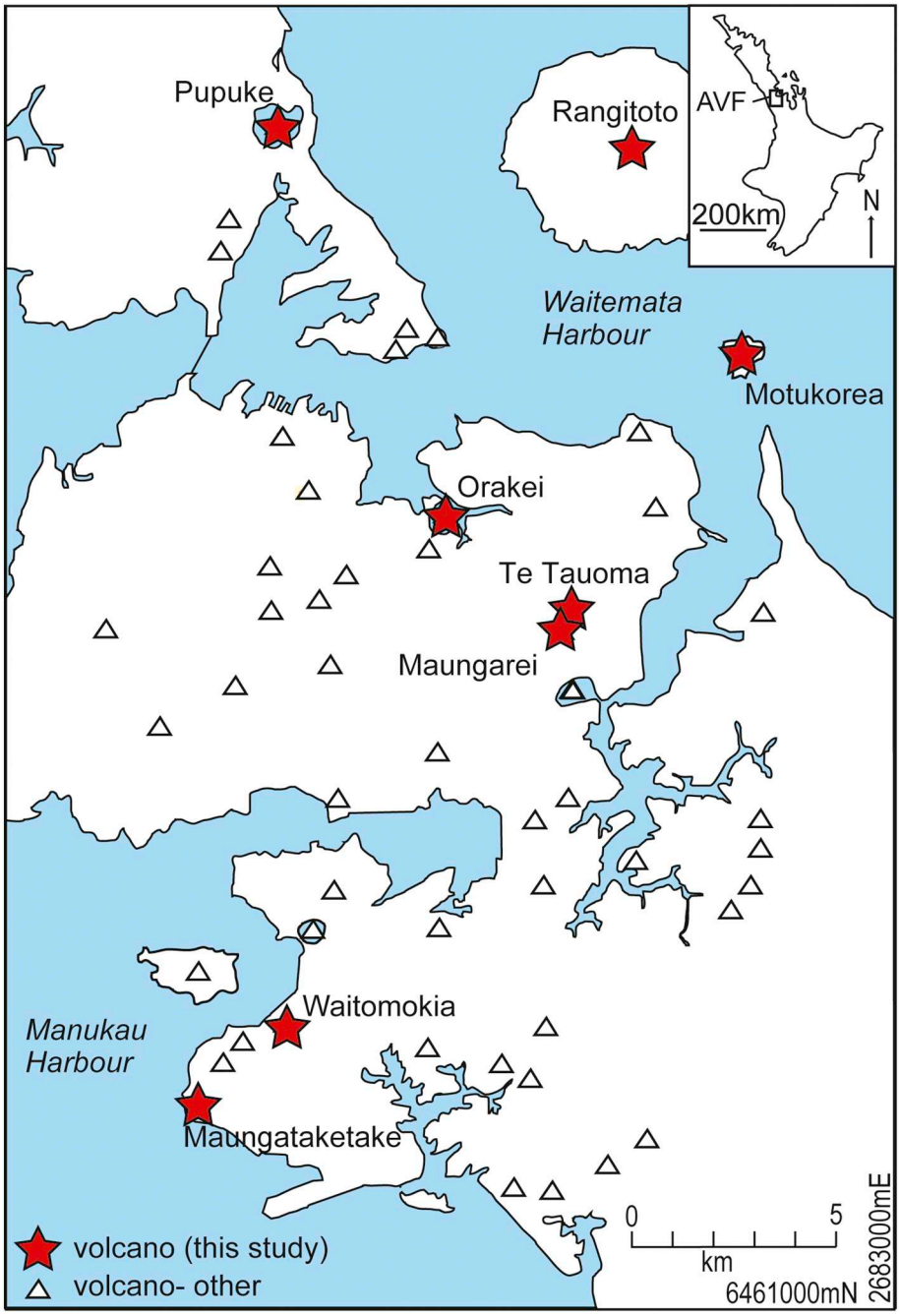

Fig. 1. Map of the Auckland Volcanic Field vent sites. Red stars indicate volcanoes analysed in this study. The volcanic field is completely encompassed within the city of Auckland. (For interpretation of the references to color in this figure legend, the reader is referred to the web version of this article.)

time of writing), is a monogenetic basaltic field comprised of ~51 eruptive centres with eruption ages from ~193 ka to 500 ybp (Leonard et al., 2017). The AVF is arguably one of the world's most intensely studied monogenetic fields (see Determining Volcanic Risk in Auckland (DEVORA) website for compilation of recent publications; www.devora.org.nz). Despite this scientific scrutiny, there is no consensus as to the driving forces of magma generation at depth. Multiple geologic processes have the potential to influence the composition and ascent of AVF magmas locally, including tectonic rifting (e.g. Hauraki Rift; Hodder, 1984), subduction-generated metasomatism (Smith et al., 1993; Huang et al., 2000), and the presence of a mantle "hot zone" (Horspool et al., 2006). The range of AVF basalt compositions supports the idea that one or more of these processes is involved in their magma generation (McGee et al., 2013).

Geochemical modelling of basalt compositions, including whole rock trace element and Pb-Sr-Nd isotope compositions, has led to multiple explanations for the compositional variability of basaltic magmatism in New Zealand (e.g. McGee et al., 2013, 2015; McCoy-West et al., 2010; Scott et al., 2016; Dalton et al., 2017). Studies of mantle xenoliths, primarily from the south island of New Zealand also indicate an isotopically heterogeneous lithospheric mantle that underwent variable degrees of metasomatism (Scott et al., 2016; McCoy-West et al., 2010; Dalton et al., 2017). In particular, it has been argued that carbonatitic metasomatism may be responsible for the trace element signature of HIMU-like basalts in Zealandia (McGee et al., 2015; Scott et al., 2016; McCoy-West et al., 2010). Alternatively, trace element and isotopic heterogeneity may be explained with a mixture of up to 3 distinct mantle sources; including lithospheric mantle, garnet-bearing

asthenospheric mantle, and discrete localized domains of ecologitized/carbonatized mantle (McGee et al., 2013; McGee et al., 2015; Wang et al., 2016). Regardless of the chosen model (variably metasomatised lithosphere versus mixing of asthenospheric and lithospheric melts), the Pb-Nd-Sr isotopic variations clearly indicate that the basalts are derived by variable melting of a heterogeneous source. In the AVF, magma compositions are, for the most part, highly silica-undersaturated and prior interpretations have suggested they experienced relatively rapid rates of ascent with minimal crustal interaction (McGee et al., 2012; Brenna et al., 2018; Hopkins et al., 2016). Os-isotopic systematics also indicate a minimal amount of crustal interaction, with only marginally elevated $^{187}Os/^{188}Os$ ratios, and no effect on other isotopic or trace element systematics (Hopkins et al., 2016).

Noble gases are key tracers of mantle reservoirs. Changes in noble gas isotopic compositions are also related to processes responsible for U, Th, and K distribution such as metasomatism (Graham, 2002; Gautheron et al., 2005). For example, significant He isotopic variability has been observed on short length scales associated with the melting of distinct mantle heterogeneities beneath the Southeast Indian Ridge, including observations of nearly the entire range of MORB (7–10 R_A) over a ~10–20 km distance (Graham et al., 2014). Melting of mantle containing small domains of heterogeneous material, such as eclogite or garnet pyroxenite, are interpreted to result in distinctly lower He isotopic compositions compared to eclogite- or pyroxenite-free mantle (Graham et al., 2014). As such, noble gases may serve as an important tool for understanding mantle chemical heterogeneity. In this study, He isotopic compositions and CO_2 abundances within olivine phenocrysts from the compositional spectrum of AVF basaltic magmas have been measured to assess the possible variations in source compositions and potential metasomatic effects. The results also provide potential insights into the regional history of the New Zealand mantle.

2. Methods

2.1. Sample selection

Twelve samples were selected from eight Auckland volcanic field centres to cover the range of isotopic compositions in AVF basalts (McGee et al., 2013). These compositions have previously been associated with diverse sources, including the lithospheric mantle (having a minor subduction component), garnet-bearing asthenospheric mantle, and an additional source that is variably ascribed to a HIMU-like component generated from melting of ecologitized or carbonatized mantle (McGee et al., 2013, 2015). Notably, the isotopic and trace element variability dictated the choice of samples for this study (Table 1). Most samples were fresh tephra containing olivine phenocrysts that were then separated by hand-picking under a binocular microscope. Three lava samples were also analysed for comparison, including a basaltic lava from the Taupō volcanic zone (Ongaroto, Onga-1; Table 2). A complete list of AVF samples and locations is available in Table 1. Samples designated with an “AU” prefix originate from the University of Auckland sample archive. Volcano names are all provided in Te Reo Maori (Browns Island/Motukorea; Mt. Wellington/Maungarei; Purchas Hill/Te Tauoma).

2.2. Olivine preparation

For lava samples (Rangitoto, Maungarei, and Ongaroto), blocks were lightly crushed and olivine grains were manually separated. Grains were relatively clean, unaltered and free of adhering groundmass. Both melt- and fluid-inclusions are evident in separated olivines. Tephra samples were first sieved to identify loose olivine crystals, then clasts were very lightly crushed to disaggregate tephra. Olivine phenocrysts were hand-picked under a binocular microscope from both tephra and lava samples. Clean samples (lacking glass or alteration on grain exteriors) primarily came from the lava samples. Tephra olivine samples included varying and significant amounts of glass adhering to grain surfaces. Tephra olivine was treated in fluoroboric acid (HBF_4) at the University of Oregon to remove adhering glass. Grains were placed in small plastic beakers and covered with HBF_4. Time in the HBF_4 ranged between 30 min and 1 h. Samples were swirled lightly every 15 min. Small grains were limited to 30 min while time for larger grains or grains with significant glass varied to optimize removal of exterior glass while reducing etching to grain surfaces. Despite the relatively short duration in HBF_4, treated olivine grains were generally more brittle than untreated grains, and usually showed a decrease in mean grain size (Fig. 2). After treatment, the samples were neutralized with Na_2CO_3 and then rinsed with water and isopropanol. All samples underwent a series of Ethanol washes in an ultrasonic bath in 5–10 min increments to remove any remaining unwanted debris, with rechecking/picking for a comprehensive removal of all surface coatings on grains. Final sample weights ranged from 0.0709 g to 0.4333 g (mean size was 0.1357 g). Two of the samples were also analysed without treatment, to provide a test of the effects of adhering glass on the measured $^3He/^4He$ ratio and the He and CO_2 concentrations.

2.3. Isotope measurements

Helium abundance and isotopic measurements on olivine were performed at Oregon State University following established methods (Graham et al., 2014). Individual samples were crushed in vacuum to extract gases trapped in fluid and/or melt inclusions within the mineral grains. CO_2 was isolated during the crushing using a liquid nitrogen cold trap, and its concentration was subsequently determined by capacitance manometry on a 1-Torr full-scale manometer (Graham et al., 2018). Sample He concentration was determined by comparison of the ^4He peak height to a calibrated volume of standard gas that was analysed routinely throughout the analytical campaign (the helium standard of Japan known as HESJ; Matsuda et al., 2002). Sample $^3He/^4He$ was determined by comparison to HESJ, which has a $^3He/^4He$ ratio of 20.4 R_A relative to marine air that was collected at the Oregon coast during 2007 (Graham et al., 2014). Line blanks were performed before sample analyses; the average ^4He blank was 2.7×10^{-11} cm^3 STP ^4He, and comprised between only 0.1 to 3.9% of the ^4He measured in the AVF sample suite (with the exception of olivine from the Taupō Volcanic Zone Ongaroto basalt, for which it was 7%). All the reported helium isotope results in this study are blank corrected.

2.4. Major and trace elements analysis

Whole rock major and trace element abundances for nine samples were measured at Washington State University following routine procedures for sample preparation and analysis via XRF and ICPMS (Johnson et al., 1999; Knaack et al., 1994). Major elements were analysed on low-dilution (3.5 g sample: 7 g dilithium tetraborate) fused glass beads on a Thermo-ARL automated XRF. Trace element analyses use a standard fusion-dilution method on an Agilent ICP-MS and are calibrated against USGS and international standards with reported long-term precision of < 5% for REE and < 10% for trace elements. Precision of measurements is based on the analysis of a replicate glass bead, with major elements better than 1% (excluding Na_2O and K_2O at 1.7 and 1.4%, respectively) and better than 4% for trace elements (excluding Cs and Pb, 10 and 20%, respectively). These analyses are augmented with three further analyses of samples AU62410; AU62438, and AU62444, from McGee (2012), covering the spectrum of proposed end-member compositions (Table 1).

3. Results

Whole rock major and trace element abundances for the tephra and lava samples are reported in Table 1. Incompatible trace element abundances show nearly an order of magnitude variation. The sub-

Table 1
Sample major element and trace element composition.

Location	Rangitoto	Rangitoto	Rangitoto	Rangitoto	Rangitoto	Lake Pupuke	Maungarei	Maungarei[a]	Motukorea[a]	Te Tauoma	Orakei	Motukorea[a]	Waitomakia	Mangataketake
Sample ID	AU59337-1	AU59337-2	MR-Rangi1	AU49951-1	AU49951-2	Pupuke7	078	AU62410	AU62444	AU62402	OB-16B-102m	AU62438	Waitomakia-Q	Mangataketake
Age (ka)[b]	0.504	0.504	0.504	0.553	0.553	193	10.3	10.3	14.3	10.9	10.9	14.3	> 15.2	88.9
Type	T	T	L	T	T	T	T	L	T	T	T	T	T	T
HBF_4	N	Y	N	N	Y	N	Y	N	Y	Y	Y	Y	Y	N
Class	SA	SA	SA	A-low	A-low	A-low	A-low	A-low	A-low	A-high	A-high	A-high	A-trans	A-trans
Normalized major elements (weight %)														
SiO_2	49.45		49.46	47.76		46.26	44.17	42.28	41.37	40.12	42.35	42.33	45.11	44.20
TiO_2	2.111		2.013	2.734		2.458	2.597	2.62	2.75	3.02	3.070	2.70	2.694	2.754
Al_2O_3	15.12		14.71	14.42		13.30	12.71	11.66	11.94	11.49	12.31	11.74	12.75	12.21
FeO*	11.35		11.53	11.64		13.34	12.85	12.51	13.04	14.80	13.81	13.08	13.35	13.12
MnO	0.167		0.168	0.175		0.185	0.193	0.19	0.22	0.24	0.208	0.22	0.199	0.195
MgO	7.95		8.55	6.93		10.39	12.10	13.18	10.64	9.69	10.15	9.97	11.44	11.08
CaO	9.49		9.38	10.76		9.58	10.60	10.72	11.58	11.39	10.60	10.94	9.43	10.85
Na_2O	3.32		3.24	3.70		3.10	2.93	3.41	4.50	4.65	4.67	3.87	3.08	3.40
K_2O	0.75		0.68	1.35		0.91	1.27	1.23	1.37	1.93	1.81	1.80	1.29	1.43
P_2O_5	0.291		0.271	0.529		0.481	0.580	0.57	0.94	1.34	1.034	1.01	0.665	0.756
Sum	99.84		100.29	98.32		99.08	99.17	98.37	99.70	99.83	98.97	99.68	99.05	99.67
LOI %	0.00		0.00	1.04		0.72	0.52			−0.07	0.48		0.97	0.00
Trace element abundances (ppm)														
La	14.17		13.16	34.38		28.36	36.74	36.94	36.16	90.65	61.73	69.73	41.81	49.61
Ce	31.80		29.86	67.66		57.02	69.49	70.61	70.28	167.3	121.3	132.3	81.65	95.71
Pr	4.24		3.96	8.24		6.93	8.70	8.36	8.15	19.32	14.30	14.92	9.67	11.38
Nd	18.57		17.44	33.24		28.12	34.73	35.08	33.15	77.15	55.38	58.30	37.61	44.51
Sm	4.88		4.72	7.35		6.33	7.27	7.11	6.70	13.81	10.99	10.61	7.73	9.14
Eu	1.72		1.66	2.41		2.16	2.45	2.22	2.18	4.27	3.52	3.29	2.52	2.97
Gd	4.96		4.95	6.83		6.05	6.76	6.18	6.15	11.82	9.16	9.05	6.84	7.97
Tb	0.81		0.78	1.03		0.90	0.98	0.85	0.81	1.46	1.27	1.15	0.99	1.15
Dy	4.63		4.68	5.61		4.93	5.42	4.74	4.74	7.78	6.36	6.10	5.38	5.93
Ho	0.88		0.86	0.97		0.87	0.95	0.85	0.80	1.25	1.04	1.04	0.91	0.99
Er	2.19		2.19	2.33		2.04	2.24	2.04	2.11	2.77	2.25	2.53	2.15	2.24
Tm	0.29		0.29	0.30		0.25	0.28	0.27	0.28	0.35	0.26	0.32	0.26	0.27
Yb	1.74		1.75	1.68		1.47	1.58	1.59	1.55	1.79	1.42	1.67	1.45	1.49
Lu	0.25		0.25	0.24		0.20	0.23	0.20	0.20	0.22	0.19	0.23	0.20	0.21
Ba	109		101	280		195	274	272	273	479	387	460	291	348
Th	1.65		1.53	4.49		3.27	3.98	4.39	4.44	10.79	7.03	9.00	4.84	6.12
Nb	15.61		14.50	52.59		38.34	49.91	57.20	55.84	116.6	80.02	96.86	55.87	69.21
Y	21.57		21.32	24.25		21.04	23.67	20.54		31.19	25.54		22.40	24.34
Hf	3.63		3.48	5.00		4.18	4.46	4.77	4.02	8.58	6.72	6.35	5.07	5.46
Ta	1.07		0.99	3.35		2.49	3.19	3.97	3.64	7.65	5.08	6.42	3.61	4.29
U	0.52		0.48	1.22		0.89	1.19	1.19	1.29	2.99	2.21	2.50	1.48	1.78
Pb	2.94		2.69	3.65		2.80	15.3	2.83	5.22	5.10	6.14	7.61	4.15	5.67
Rb	11.5		10.8	23.8		13.7	20.7	22.0	19.4	33.7	31.8	33.1	22.5	26.6
Cs	0.43		0.41	0.62		0.27	0.35	0.27	0.25	0.45	0.55	0.58	0.40	0.55
Sr	371		348	583		510	602	592	572	1212	942	942	638	752
Sc	24.7		24.9	24.3		21.8	23.3	25.7	26	20.1	17.5	21	20.0	19.9
Zr	146		137	209		176	188	214	318	371	313	355	226	238

[a]Compositions from McGee (2012). [b]Ages from Leonard et al. (2017). Type T (tephra) and L (lava). Basalts are classifed subalkaline/alkaline with alkaline subdivided into low-, high-, and transitional-based on La/Yb[N] as discussed in the text.

Table 2
He isotopic composition and CO_2 and He abundances in olivine.

Volcano	Sample ID	Tephra/Lava	Treated	Mass (g)	$^3He/^4He$ (R/R_A)	2-sigma	[He] (cm^3 STP/g)	[CO_2] (cm^3 STP/g)	$CO_2/^3He$
Rangitoto	AU59337-1	T	N	0.4333	6.79	0.18	3.19E−08		
Rangitoto	AU59337-2	T	Y	0.1012	7.15	0.16	1.12E−07	0.0012	1.08E+09
Rangitoto	MR-Rangi1	L	N	0.1747	7.02	0.16	6.92E−08	0.0021	3.11E+09
Rangitoto	AU49951-1	T	N	0.1255	7.26	0.17	1.27E−07		
Rangitoto	AU49951-2	T	Y	0.1081	7.26	0.16	9.76E−08	*0.00051*	5.18E+08
Lake Pupuke	Pupuke7	T	N	0.1172	6.57	0.37	1.21E−08	0.00078	7.06E+09
Maungarei	078	T	Y	0.1192	7.08	0.17	6.79E−08	0.0014	2.10E+09
Maungarei	AU62410	L	N	0.2763	6.72	0.23	1.77E−08	0.00056	3.39E+09
Motukorea	AU62444	T	Y	0.2647	6.96	0.22	1.73E−08	*0.00014*	8.36E+08
Te Tauoma	AU62402	T	Y	0.0887	7.24	0.23	5.07E−08	*0.00031*	6.08E+08
Orakei	OB-16B-102m	T	Y	0.1275	7.22	0.13	1.77E−07	*0.00038*	2.14E+08
Motukorea	AU62438	T	Y	0.0709	7.19	0.17	1.39E−07	*0.00013*	9.36E+07
Waitomakia	Waitomakia-Q	T	Y	0.1438	7.33	0.19	6.09E−08	*0.00044*	7.09E+08
Mangataketake	Mangataketake	T	N	0.2436	7.48	0.14	7.62E−08	0.00056	7.07E+08
Ongaroto	Onga-1 (TVZ)	L	N	0.1780	5.27	0.52	2.81E−09	0.00051	2.48E+10

The $^3He/^4He$ ratio (R) is reported relative to the atmospheric ratio (R_A) of 1.39×10^{-6}.
Italicized [CO_2] results indicate that the measured pCO_2 was < 1 mtorr.
Onga-1 is a basalt from the Taupo volcanic zone (TVZ) analysed for comparision to the Auckland volcanic field basalts.

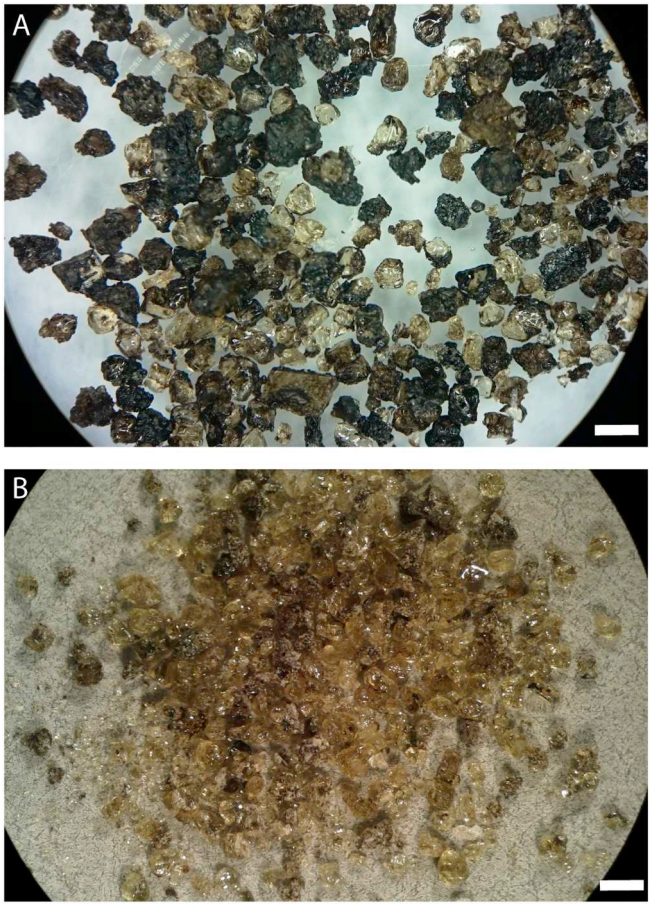

Fig. 2. Microscope images of sample AU59337, Rangitoto subalkaline tephra, before (A) and after (B) HBF_4 treatment. The white scale bar is 1 mm.

alkaline Rangitoto lava and tephra are distinct outliers compared to the other alkaline, silica-undersaturated basaltic samples (Fig. 3). Collectively, alkaline tephras and lavas have similar trace element and REE patterns, albeit with varying degrees of enrichment at similar MgO contents (Fig. 3; Table 1). The alkaline magmas are characterized by a distinctive enrichment in Nb and Ta and although variable, a relative depletion in Pb (Fig. 3a). REE distribution is used here to categorize the basalts for later discussion (Fig. 3b). For example, the chondrite-normalized ratio of La/Yb ($La/Yb_{[N]}$) ratio can be affected both by the presence of garnet during melting (due to the compatible behaviour of HREEs) and by differences in source enrichment and/or degree of melting (which can lead to larger relative variations in the LREEs). Subalkaline magmas in the AVF have characteristically low $La/Yb_{[N]}$ of ~5, while alkaline magmas have $La/Yb_{[N]}$ between 13 and 35. The alkaline magmas can be further subdivided, with $La/Yb_{[N]}$ forming two main clusters from ~13–15 and ~28–35, with several transitional samples having $La/Yb_{[N]}$ of ~19–22. This clustering of compositions is consistent with previously defined "endmember" isotopic compositions for the AVF (McGee et al., 2013).

New CO_2 and He results are reported in Table 2. The He concentrations in olivine from the Auckland volcanic field range from 1.8×10^{-7} to 1.1×10^{-8} cm^3 STP/g (Fig. 4). Despite the factor of 16 variation in [He], the $^3He/^4He$ ratios (R_A) for the 14 samples lie in a very narrow range from 6.6 to 7.5 (mean = 7.10 ± 0.26 1σ; Fig. 4).

Despite the young age of erupted basalts (< 193 ka; Leonard et al., 2017), the high abundances of U and Th (up to 3 ppm and 10.8 ppm, respectively) make the initial amount of trapped magmatic He and its isotopic compositions potentially susceptible to contamination by post-eruptive radiogenic ^4He. Assuming that a minimum mass proportion of 10% degassed glass was present for our olivine mineral separates, closed system post-eruptive production of ^4He would result in a decrease in $^3He/^4He$ of < 0.1 R_A given the measured amounts of ^4He that were released by crushing. Therefore, any post-eruptive addition of radiogenic He to the measured $^3He/^4He$ in these samples is negligible.

Replicate analyses (HBF_4-treated and untreated) of the Rangitoto volcano tephra showed no systematic effect on $^3He/^4He$ between treated (to remove adhering glass) and untreated analyses (Fig. 5). Sample AU49951 has an identical $^3He/^4He$ of 7.26 R_A, regardless of treatment, but slightly different He concentrations of 9.8×10^{-8} cm^3 STP/g (treated) vs, 1.3×10^{-7} cm^3 STP/g (untreated). In contrast, sample AU59337 has a $^3He/^4He$ of 6.79 ± 0.18 R_A (untreated) vs. 7.15 ± 0.16 R_A (treated). In this case, the untreated sample had a significantly lower He concentration (3.2×10^{-8} cm^3 STP/g) compared to the treated sample (1.1×10^{-7} cm^3 STP/gHe). This suggests that the effects of a small amount of adhering glass on the olivine is not systematic (Fig. 5b). In some cases its presence may dilute the analysed sample mass with degassed material that contains little, if any, helium (AU49951). In other cases it may contribute some radiogenic helium, but its influence on the helium isotope ratio is barely detectable (AU59337). It is also possible that variability in the amount of helium trapped within olivine phenocrysts for individual basalts is a contributing factor when comparing treated and untreated samples (AU59337).

In contrast to younger volcanics, for the oldest sample (Lake

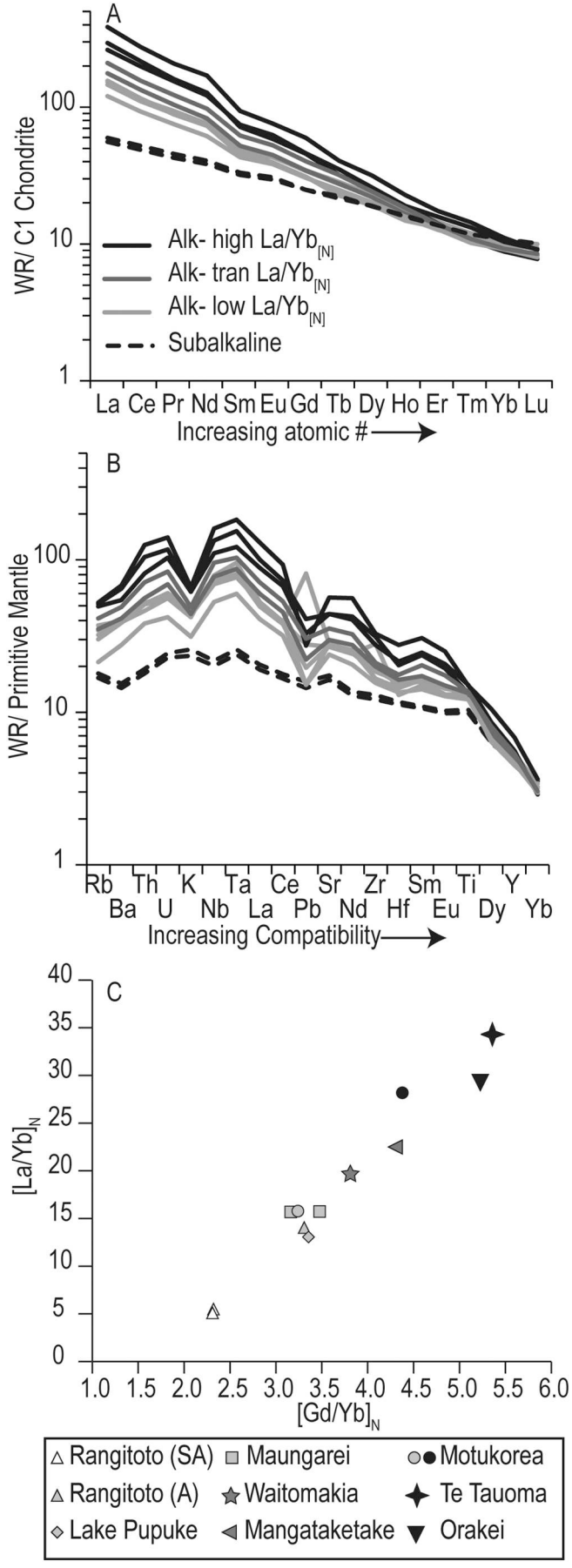

Fig. 3. Whole rock rare earth element (A) and trace element (B) distributions in tephras and lavas (data from this study and McGee, 2012) normalized to C1 chondrite and primitive mantle, respectively (Sun and McDonough, 1989; McDonough and Sun, 1995). (C) Chondrite normalized REE ratios used for classification as in text, subdivided into alkaline and subalkaline compositions, with alkaline magmas categorized based on $La/Yb_{[N]}$. Shading, from light grey, to dark grey, to black corresponds with increase LREE and MREE enrichment for low-, transitional-, and high-alkali enriched basalts.

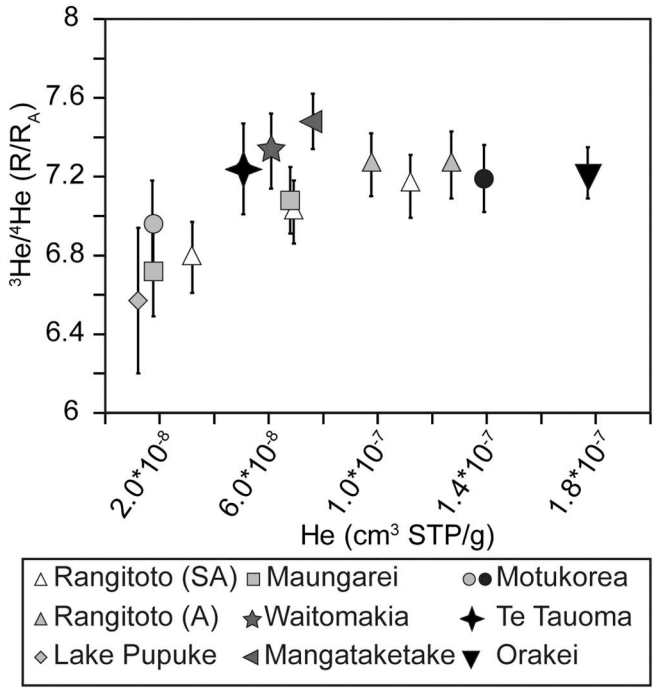

Fig. 4. $^3He/^4He$ (R/R_A) for AVF olivine versus olivine trapped He content (cm^3 STP/g).

Pupuke, 193 ka; Leonard et al., 2017), 10% contamination by post-eruptive radiogenic helium from adhering glass would lead to the addition of 1.6×10^{-8} cm^3/g ^4He and a potential downward shift in $^3He/^4He$ by 1.6 R_A. Depending on the amount of magmatic helium that was trapped in the olivine, volcanic glass coating this sample may constitute a more significant proportion by mass. Therefore, the HBF_4 cleaning procedure is recommended for glass-coated tephra in somewhat older samples such as this one.

In addition to the treated-untreated comparison, our results allow a comparison between co-existing lava and tephra samples (Fig. 5). Treated olivine from tephra AU59337 compared to co-existing subalkaline lava (Rangi-1) have indistinguishable $^3He/^4He$ ratios of 7.15 ± 0.16 R_A and 7.02 ± 0.16 R_A, respectively. The Maungarei tephra (078) and lava (AU62410) show a slight difference in $^3He/^4He$ (7.08 ± 0.17 R_A and 6.72 ± 0.23 R_A, respectively). Helium abundances are systematically higher in olivine from tephra samples compared to those from lava flows. Although the results are somewhat variable, they suggest that treating of glass-coated olivine from tephra in HBF_4 helps to increase the yield of He (cm^3 STP/g) when significant exterior glass is present, and may result in slightly higher measured $^3He/^4He$ ratios (Fig. 5). Although an appreciable difference in $^3He/^4He$ between lava and co-genetic tephra is absent, the He concentration yields appear to be elevated for treated tephra olivine compared to untreated olivine from lava flows that has minimal adhering groundmass. For consistency, going forward in the discussion we only incorporate treated, or glass-free, tephra and lava olivine separates.

The crushed CO_2 concentrations vary by magnitude factor of 16 (similar to He), and range from 1.3×10^{-4} to 2.1×10^{-3} cm^3 STP/g

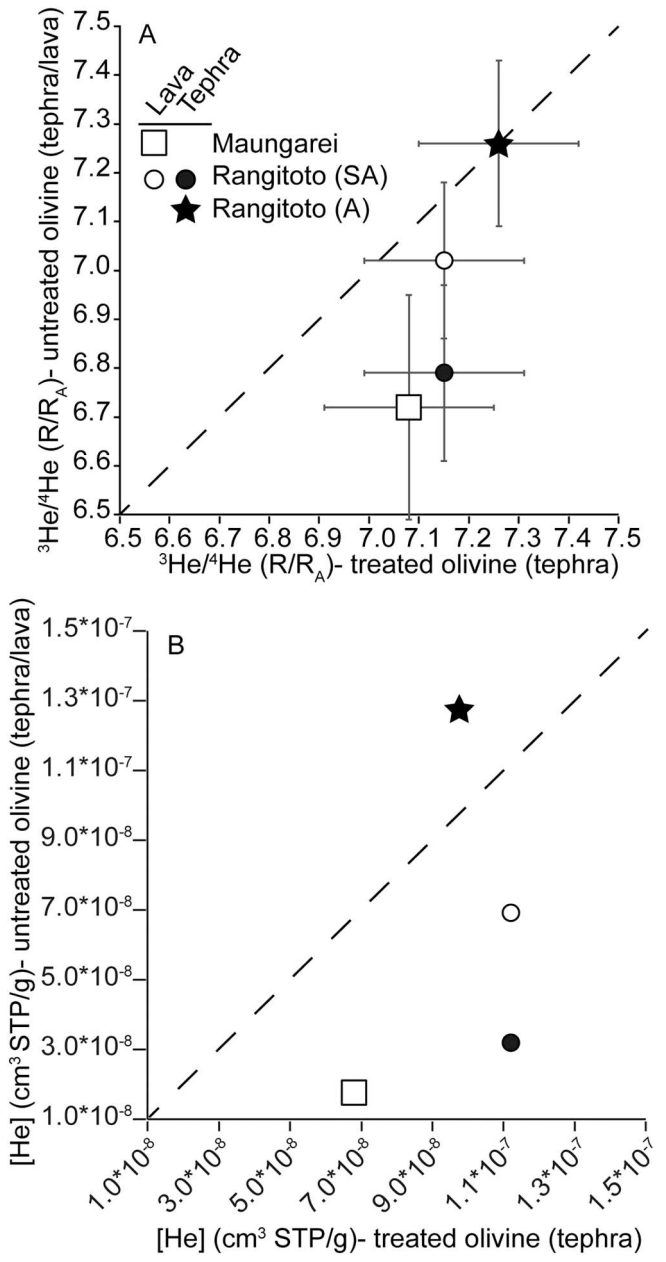

Fig. 5. Comparison between (A) ^{3}He/^{4}He (R/R$_A$, where R is the measured ratio and R$_A$ is the atmospheric value of 1.39 × 10^{-6}), and (B) He (cm^3 STP/g) for HFB$_4$-treated Rangitoto olivine and untreated "glassy" subalkaline (black circle), alkaline (black star) olivine from the same samples. In addition, open symbols represent treated olivine versus olivine from lava (untreated) for Rangitoto subalkaline lava (open star), and Maungarei lava (open square). Error bars are 2σ.

(Table 2). As noted in Table 2, when our measured pCO_2 is < 1 mtorr, analytical uncertainties are generally significantly larger. This is because any small drift in the manometer baseline during the time required for sample processing (about 30 min) could introduce some uncertainty. At this level (< 1 mtorr), the pressure measurement can only made to 1 significant figure (i.e., 0.1–0.9 mtorr). Analytical uncertainties on samples having pCO_2 < 1 mtorr are therefore probably close to 10%. In addition, CO_2 concentrations are not available for untreated tephra samples because in these cases the pCO_2 was near the detection limit (≤0.2 mtorr). The measured [CO_2] in olivine from the Maungarei lava (AU62410, 0.0056 cm^3/g) is 2.5 times lower than in the coexisting tephra (078, 0.0014 cm^3/g; Fig. 5), and shows the same depletion trend as in [He] in these two samples. In contrast, despite the larger [He] for olivine from the Rangitoto tephra (AU59337) relative to the lava-hosted olivine (MR-Rangi1), the [CO_2] is depleted by nearly a factor of 2. In general, [CO_2] does not correlate with [He] or ^{3}He/^{4}He.

Neither the isotopic composition nor abundance of He is correlated with the whole rock chemical or Sr-Nd-Pb isotopic compositions (Fig. 6a-b; McGee et al., 2013). However, CO_2 concentrations are negatively correlated with whole rock incompatible trace elements, excluding HREEs (Fig. 6c-f). The range of CO_2/He ratios in all samples varies from 9.4 × 10^2 to 6.4 × 10^4 (9.4 × 10^7 to 6.4 × 10^9 for CO_2/^{3}He, respectively) and shows no correlation with ^{3}He/^{4}He (Fig. 7). There does appear to be a weak correlation between CO_2/^{3}He and La/Yb$_{[N]}$, however it is driven almost entirely by the variation in olivine [CO_2] (Fig. 7).

4. Discussion

4.1. Mantle drivers of [CO_2] and [He] variations

The anti-correlation between whole rock trace elements (e.g. U, La, Zr) and ratios (e.g., La/Yb) and trapped CO_2 content of olivine, and by extension CO_2/^{3}He, suggests the involvement of a magmatic process and/or a mantle source control (Figs. 6, 7). This relies on the assumption that the amount of trapped CO_2 in the olivine is proportional to the amount of CO_2 in the magmatic system (melt + exsolved volatiles) at the time of olivine crystallization. Due to its incompatibility, the concentration of CO_2 in the melt will vary inversely with the degree of melting. As described above, La/Yb may serve as a useful discriminant for degree of partial melting as well as a tracer of magmatic end-members and their mantle sources (McGee et al., 2013; Scott et al., 2016). The co-variation between melt trace element chemistry and CO_2 concentrations may relate to variations in initial CO_2 in a heterogeneous mantle source. This would imply that the most trace element-enriched basalts are derived from a mantle source that has the lowest CO_2, while subalkaline basalts are derived from a CO_2-rich mantle source. This scenario seems unlikely based on prior geochemical models of trace elements and isotopes that suggest the trace-element enriched alkali basalts are derived from a mantle metasomatised by a volatile (carbonate)-rich low-degree melt from the asthenosphere (e.g. McGee et al., 2015; McCoy-West et al., 2010; Scott et al., 2016).

While a heterogeneous mantle is required to explained the observed Pb-Nd-Sr and Mg isotopic variability (e.g. Cook et al., 2005; Hoernle et al., 2006; Wang et al., 2016; McCoy-West et al., 2010), differences in the extent of partial melting combined with mixing accounts for much of the La/Yb variation in AVF basalts (McGee et al., 2013). The high-La/Yb$_{[N]}$ alkali basalts in the AVF have been proposed to originate as low-degree (< 1%) partial melts compared to the subalkaline magmas originating from ~3% partial melting (McGee et al., 2013). The [CO_2] trapped in olivine of subalkaline samples lies between 0.0012 and 0.0021 cm^3/g (2.4 to 4.1 ppm CO_2) while in alkaline samples it shows lower values and a larger range, between 0.00013 and 0.0014 cm^3/g (0.3 to 2.8 ppm CO_2). CO_2 solubility is greater in alkali basalts compared to subalkaline compositions (Dixon, 1997), and as a result, if olivine crystallization occurs at approximately the same pressure for both basalt types, then the alkali basalts should retain higher CO_2 melt contents, even if they experience deeper saturation and some gas loss (Hartley et al., 2014). Thus, the inverse correlation between trace elements and CO_2 abundance is opposite to what would be observed if the degree of partial melting is the sole control on CO_2 and trace element variability (Fig. 7c). This partial melting scenario is only viable if early saturation of CO_2 results in a more efficient separation of fluid/vapour phase (bubbles) from the melt, thus significantly reducing a CO_2-rich component from the melt + fluid magmatic system prior to olivine crystallization and entrapment of volatiles (Hartley et al., 2014). Alternatively, we must consider the possibility that [CO_2] and [He] are unrelated to the mantle source and are instead related to magmatic processes after olivine crystallization.

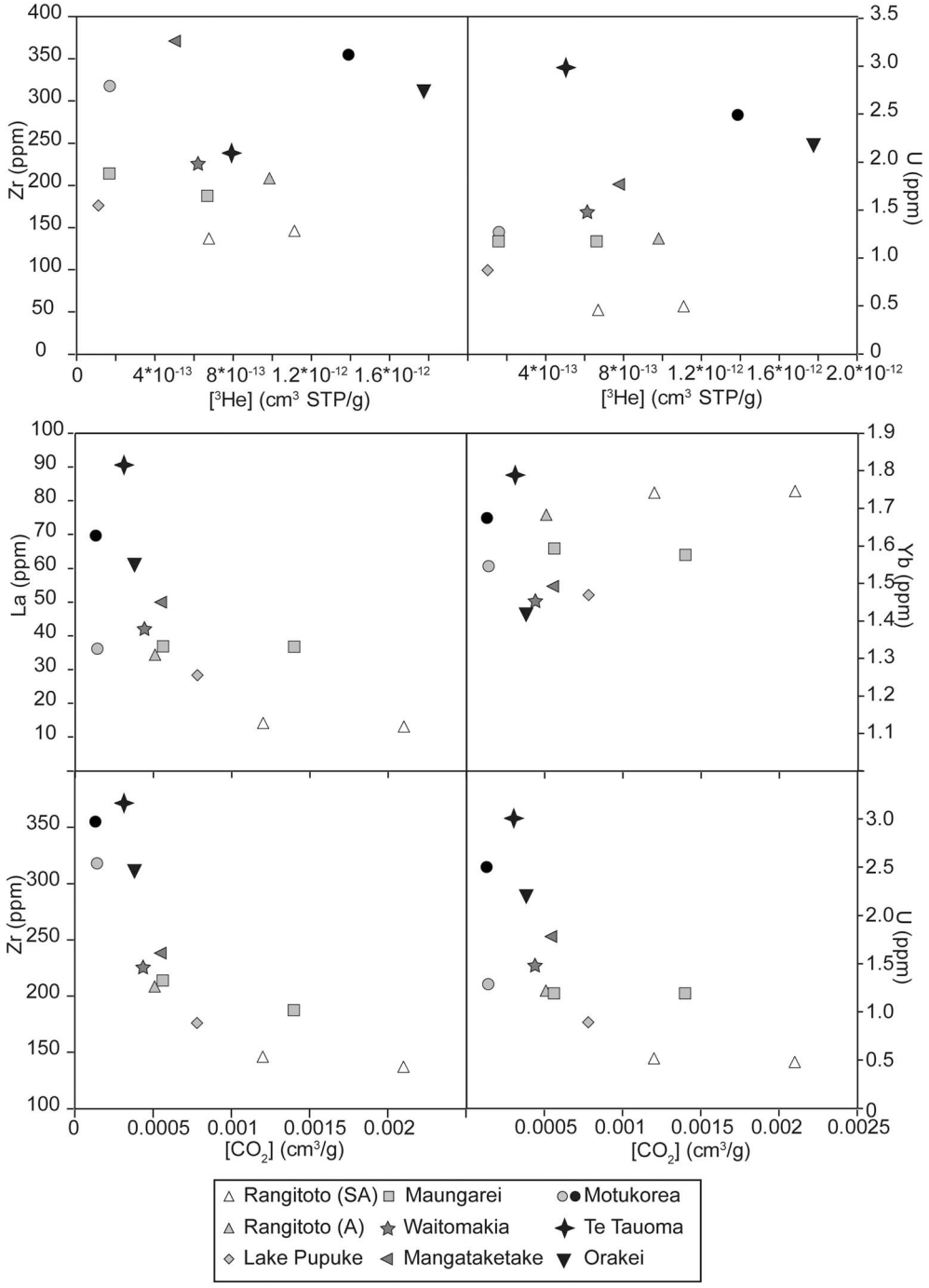

Fig. 6. Whole rock trace element abundances versus (a-b) He abundances and (c-f) CO_2 abundances. Note that the Lake Pupuke sample is predominantly composed of xenocrystic olivine but for the purposes of this study, gas chemistry from olivine is plotted versus its whole rock composition.

4.2. Post-crystallization mechanisms for variations in [CO_2] and [He]

The gas concentrations in olivine released by crushing, and potentially the ratios of volatile elements, depend on the ability of olivine to trap both melt and fluid (i.e. CO_2-rich bubbles that may be present in the magma at depth). The variations in He and CO_2 concentrations measured by crushing of AVF olivines could be influenced, therefore, both by volatile exsolution into vapour (shrinkage) bubbles after melt inclusion entrapment, and the amount of fluid (number of fluid inclusions) trapped from a vapour-saturated melt. Recent studies have highlighted the significance of gas (CO_2) in vapour shrinkage bubbles associated with melt inclusions (Moore et al., 2015; Tucker et al., 2019). Measurements of shrinkage bubble volumes from Hawaiian volcanoes show a maximum frequency at only 3–4 vol% (predominantly < 8 vol%), but there are some outliers at > 20 vol% (Tucker et al., 2019).

Given the lower solubility of CO_2 compared to He in basaltic melts (Tucker et al., 2018; Graham et al., 2018), a melt inclusion may undergo CO_2/He fractionation following its entrapment and the formation of shrinkage bubbles. This should lead to a higher CO_2/He in the gas phase (shrinkage bubble) compared to what is left dissolved in the melt inclusion. Kinetic (diffusive) fractionation might produce an opposing effect on the CO_2/He ratio, depending on the relative diffusion rates of He and CO_2 compared to the cooling/quenching rate of the melt

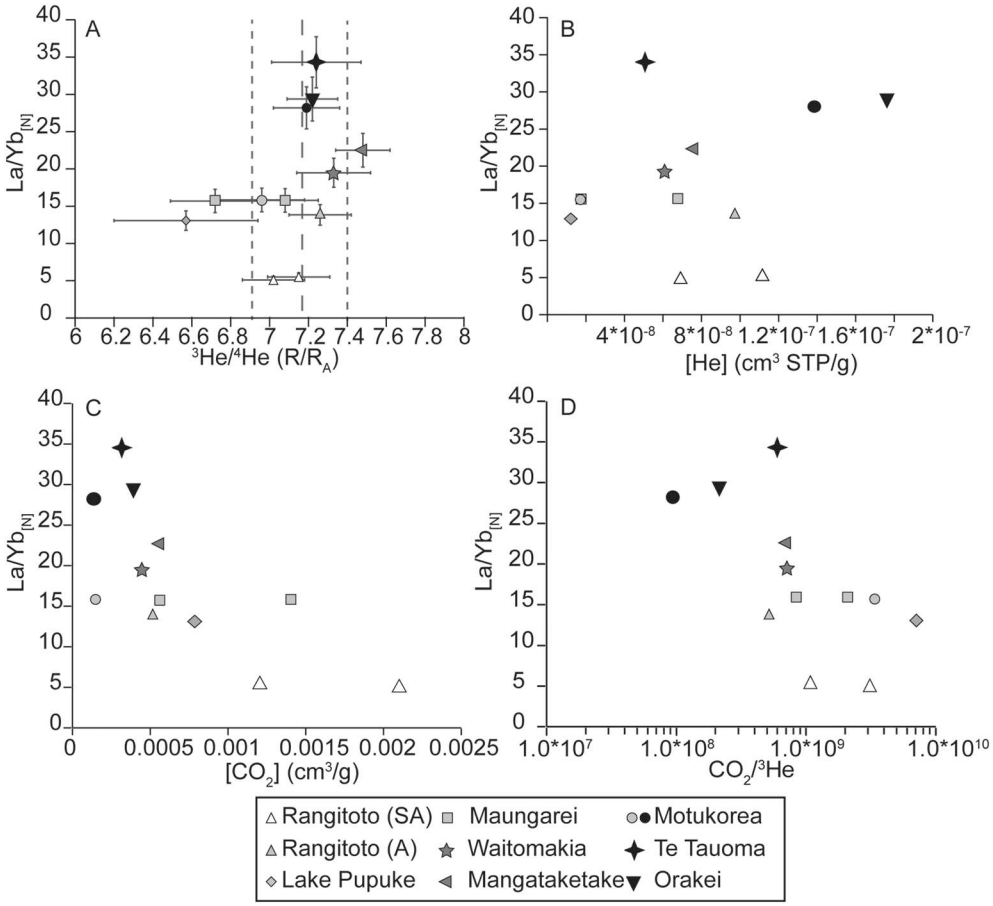

Fig. 7. Chondrite Normalized (McDonough and Sun, 1995) whole rock La/Yb versus (A) $^3He/^4He$, (B) trapped He content of olivine, (C) trapped CO_2 content of olivine, and (D) $CO_2/^3He$. Error bars for La/Yb are included in panel (A). Long and short dashed lines in (A) represent the average (long-dash) and 1std dev (short dash) for AVF phenocrysts. The light grey diamond represents a potential xenocrystic sample (Lake Pupuke; Brenna et al., 2018), however is plotted based on whole rock $La/Yb_{[N]}$. Symbols and shading are the same as in Fig. 3.

inclusion. To quantitatively characterize the role of shrinkage bubbles in melt inclusions trapped in olivine relative to fluid inclusions that were directly trapped from magma would require a knowledge of shrinkage bubble and fluid inclusion volumes, the relative densities of CO_2 and He, and the distribution of the inclusions through a bulk olivine separate. Based on X-ray computed tomography coupled with single crystal gas analysis for CO_2 and He in Samoan olivines, Horton et al. (2019) argued that He is primarily stored in fluid inclusions. However, melt inclusions were not taken into account in that study due to limitations in image resolution. Notably, the He concentration correlated broadly with fluid inclusion density but CO_2 concentration was uncorrelated in the Horton et al. (2019) study, suggesting that there may have been a secondary CO_2 source. Therefore, the proportion of shrinkage bubbles in melt inclusions relative to trapped fluid inclusions may be a factor in controlling the CO_2 abundance and CO_2/He ratio measured by crushing olivine mineral separates. If the CO_2 abundance measured in crushed olivine is a combination of melt- plus fluid inclusion components, then why is CO_2 anticorrelated with $La/Yb_{[N]}$ and incompatible trace elements in the AVF basalts (Figs. 6 and 7)?

One possibility is that more enriched melts (e.g., as indicated by La/Yb) have a lower tendency to develop shrinkage bubbles in melt inclusions, leaving a larger proportion of CO_2 dissolved in the glass (and which may not be released during crushing). The development of shrinkage bubbles is largely a function of decreasing pressure and temperature, from inclusion trapping conditions down to the glass transition temperature, resulting both from post-entrapment crystallization of melt inclusions, and the relative difference in thermal contraction between the melt and host crystal (e.g. Roedder, 1979; Danyushevsky et al., 2002; Wallace et al., 2015). However, it is also suggested that shrinkage bubble formation is time dependent, such that faster cooling leads to less bubble development (Roedder, 1979). This means that the amount of CO_2 exsolving from the melt to the shrinkage bubble is time dependent, and strongly a function of H-loss from trapped melt inclusions (Gaetani et al., 2012; Bucholz et al., 2013). If we make a simplifying assumption that trace element enriched, SiO_2 depleted (alkaline) melts ascend more rapidly (Kokandakar et al., 2018), then shrinkage bubble growth in olivine should be reduced in high $La/Yb_{[N]}$ magmas. A priori one expects that slower magma ascent rates following olivine crystallization at depth would lead to more CO_2 exsolved into melt inclusion shrinkage bubbles, relative to faster ascending magmas. However, this effect may be partially mitigated by decreasing viscosity in low-SiO_2 (alkaline) melts, which should promote faster bubble growth (Roedder, 1979). In addition, qualitative petrographic observations of Rangitoto alkali and subalkaline basalts suggest there is no appreciable difference in the amount or size of shrinkage bubbles between the two magma compositions.

In contrast to CO_2, there is no correlation of He concentration with trace element composition or ratios of incompatible elements in AVF basalts (Fig. 6); as noted above, the variation in CO_2 concentration controls the trend between $La/Yb_{[N]}$ and $CO_2/^3He$ (Fig. 7). Although helium shows a comparable range of variability to CO_2 in our study, the absence of a correlation between their concentrations might result from partial equilibration of He with the host melt after olivine crystallization (Horton et al., 2019). We cannot quantitatively evaluate the potential diffusive loss of He after entrapment with the presently available data. However, it is notable that the He concentrations trapped in olivine of lava and tephra from the same volcano are similar (Fig. 5). Since lava and tephra are associated with dramatically different cooling rates, this similarity suggests any post-entrapment re-equilibration of He must have primarily occurred prior to eruption.

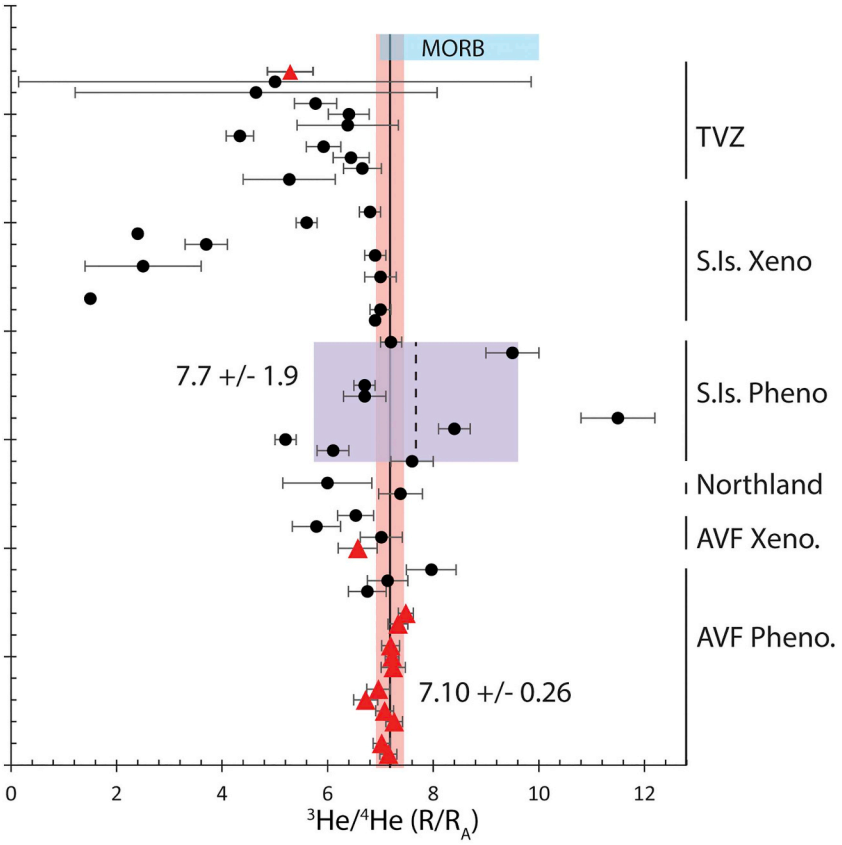

Fig. 8. $^{3}He/^{4}He$ (R/R_A) for New Zealand basalts and mantle xenoliths. Data from this study indicated by red triangles. Literature data for the Taupō Volcanic Zone (TVZ), South Island basalts and xenoliths, Northland, and the AVF in black (Patterson et al., 1994; Hoke et al., 2000). (For interpretation of the references to color in this figure legend, the reader is referred to the web version of this article.)

4.3. Significance of $^{3}He/^{4}He$ to the Origin of the AVF

The $^{3}He/^{4}He$ ratios of Auckland Volcanic Field magmas show a uniform composition of 7.10 ± 0.25 R_A, despite significant major- and trace-element compositional differences (Figs. 3, 4, 6). Prior He isotope analyses for 3 different volcanoes/samples in the AVF (Wiri, Puketutu, and Crater Hill) seem to indicate a wider range in composition but still show a similar average of 7.28 ± 0.62 R_A (Fig. 8; Patterson et al., 1994). Crustal interaction, particularly for the alkaline magmas, appears to be limited, with low $^{187}Os/^{188}Os$ (indicating less the 1%; Hopkins et al., 2016) and an olivine $\delta^{18}O$ of 5.3 ± 0.6 (Coote et al., 2019) for the Auckland Volcanic Field. Ascent rate models for AVF magmas from trace element and hydrogen diffusion in xenocrystic mantle olivine suggest relatively long residence times in the mantle (up to a year), followed by relatively rapid (< week) ascent through the crust (Brenna et al., 2018). The absence of prolonged crustal storage for AVF magmas would reduce the likelihood of significant crustal contamination.

Any attempt to account for the He isotope composition of the mantle underlying the Auckland volcanic field must address the key observation that it has low (~7 R_A) and uniform $^{3}He/^{4}He$, despite the trace element and isotopic heterogeneity observed in the AVF basalts (McGee et al., 2013, 2015). This He isotope composition lies at the boundary between most mid-ocean ridge basalts (7–10 R_A) and most lavas and xenoliths derived from the sub-continental lithospheric mantle (SCLM 5–7 R_A; Porcelli et al., 1992; Reid and Graham, 1996; Gautheron and Moreira, 2002; Dunai and Porcelli, 2002). Given the complex tectonic history of New Zealand over the last ~100 my (e.g. Mortimer, 2004; Jiao et al., 2014; Seebeck et al., 2014), it is not surprising that metasomatic enrichment in the upper mantle beneath New Zealand has occurred either from intra-mantle trapped melts or subduction modification (e.g. Huang et al., 2000; Scott et al., 2016). This metasomatised mantle may serve as the source of slightly more radiogenic He isotope compositions compared to depleted mantle. For example, the metasomatised subcontinental lithospheric mantle beneath Europe shows $^{3}He/^{4}He$ ratios of 6.5 ± 0.7 R_A, overlapping with the observed range in the AVF. However, individual localities generally show a greater helium isotope diversity (6.22 ± 0.44 R_A and 6.42 ± 0.45 R_A for Dreiser Weiher and Massif Central localities; Gautheron et al., 2005), compared to the AVF (Fig. 8). This is supported by our analysis of Lake Pupuke xenocrystic olivine (Table 2) as well as literature data of AVF olivine xenocrysts (Fig. 8; Patterson et al., 1994) which have a combined average of 6.47 ± 0.50 R_A, consistent with the global average for subcontinental lithospheric mantle. Xenocrystic olivine may be derived during magma ascent from the lithospheric mantle or Dun Mountain Ophiolite Belt underlying Auckland, however spinel inclusion compositions from Lake Pupuke olivine suggest a lithospheric mantle source (Brenna et al., 2018). A statistical *t*-test comparing the xenocrystic and phenocrystic olivine from this study and from Patterson et al. (1994) returns a *p*-value of 0.064, indicating that the xenocrystic olivine is distinguishable from the phenocrystic olivine at > 90% confidence level. This further suggests that lithospheric mantle-derived olivine on average has a higher proportion of radiogenic helium compared to most of the phenocrystic olivine of the AVF.

In addition to Mesozoic subduction and accretion events responsible for the construction of Zealandia (e.g. Mortimer, 2004; Jiao et al., 2014), tectonic models suggest the upper mantle beneath the AVF could have experienced subduction-derived metasomatism from 30 to 15 Ma (Huang et al., 2000), and as recently as 8 Ma (Seebeck et al., 2014). The He isotopic range in subduction-related magmas has long been explained as a mixture between MORB-like He ($^{3}He/^{4}He$ = 7–10 R_A) and radiogenic He (< 0.1 R_A) derived from the crust or lithosphere (e.g. Poreda and Craig, 1989; Porcelli et al., 1992; Hoke et al., 2000; Hilton et al., 2002). Notably, young subduction-derived basalts of the Taupō Volcanic Zone, including a new analysis at 5.7 ± 0.27 R_A, have systematically lower $^{3}He/^{4}He$ of 5.7 ± 0.8 R_A (Fig. 8; Patterson et al.,

1994) compared to the AVF, and are similar to the global arc mean of 5.4 ± 1.9 R_A (Hilton et al., 2002).

Prior trace element and isotopic (Sr-Nd-Pb) modelling suggested a significant role for the shallow upper mantle (up to 80% subduction-modified spinel lherzolite) for the origin of AVF basalts, particularly in the generation of higher degree partial melt basalts, such as Rangitoto volcano subalkaline compositions (McGee et al., 2013). Only a very weak enrichment of fluid mobile trace elements is evident in AVF subalkaline basalts compared to alkaline compositions, with average Ba/Nb and U/Nb at 7 and 0.033, and 5 and 0.024, respectively (Fig. 3). Despite the potentially significant role for a compositionally distinctive, metasomatised shallow upper mantle in the generation of the AVF basalts, subalkaline He-isotope compositions (treated-tephra and lava) range only from 7.02 to 7.16 R_A (7.10 ± 0.25 R_A). This range just overlaps with the least radiogenic values observed in volcanic arcs globally (Hilton et al., 2002) and is less radiogenic than olivine xenocrysts from the mantle lithosphere (Fig. 8; Patterson et al., 1994). The AVF alkaline magmas, interpreted as deeper, lower-degree partial melts (McGee et al., 2015), have identical $^3He/^4He$. A low-velocity seismic anomaly at ~80–100 km depth beneath the AVF suggests the presence of a localized thermal or compositional anomaly, and provides a potential source region for basaltic magmatism (Horspool et al., 2006). Alternative explanations for New Zealand intraplate magmatism, distributed across the North and South Islands, have suggested alkaline magmas are partially or entirely derived from a metasomatised lithospheric mantle (e.g. Cook et al., 2005; Finn et al., 2005; Panter et al., 2006; Sprung et al., 2007; Scott et al., 2016). Regardless of their mantle domain, while a slight influence from subduction-related processes is possible for the subalkaline magmas based on $^{87}Sr/^{86}Sr$ and fluid-mobile trace element enrichments, such enrichments are absent in the alkaline magmas. Subduction-related metasomatism of the upper mantle therefore cannot readily account for the uniform $^3He/^4He$ amongst the range of AVF magma compositions.

New Zealand resides within the so-called HIMU province of the SW Pacific (e.g. Woodhead, 1996; Panter et al., 2006; McCoy-West et al., 2010; Scott et al., 2014) The domain is isotopically characterized by mixing between HIMU- FOZO- EMI-EMII mantle end-members (Hart et al., 1992; Finn et al., 2005; Hoernle et al., 2006). Studies have long debated the origin of this mantle domain, and in particular the HIMU component, and primarily have suggested either a metasomatised subcontinental lithospheric mantle (SCLM) or a sub-lithospheric source (e.g. Panter et al., 2006; McCoy-West et al., 2010; Scott et al., 2014; Wang et al., 2016; Park et al., 2019). HIMU basalts have characteristically elevated $^{206}Pb/^{204}Pb$ compared to other oceanic basalts due to a time-integrated elevated U/Pb ratio in the mantle source. HIMU basalts also have low $^3He/^4He$ ratios that overlap with the low end of the range in typical mid-ocean ridge basalts derived from the upper mantle (~5.8–7.0 R_A: Graham et al., 1992; Hanyu and Kaneoka, 1997; Hanyu et al., 2014), consistent with a mantle source that also has elevated (U + Th)/He. Despite the AVF $^3He/^4He$ ratios of ~7 R_A in AVF lava and tephra that have OIB-like trace element concentrations, and the prevalence of HIMU basalts throughout the SW Pacific that include the South Island of New Zealand (e.g. Hoke et al., 2000; McCoy-West et al., 2010), these young AVF basalts lack the characteristic $^{206}Pb/^{204}Pb$ enrichment of HIMU domains (McGee et al., 2013). Instead, the AVF basalts resemble the FOZO or C isotopic mantle endmember (Hart et al., 1992; Hanan and Graham, 1996) closely overlapping with, or similar to, the compositional range of basalts from the Antarctic Peninsula, Victoria Land, and Balleny and Scott Islands (Finn et al., 2005; Park et al., 2019). The AVF also overlaps basalts from Australia and Tasmania that generally have a lower $^{206}Pb/^{204}Pb$ compared to New Zealand (Finn et al., 2005).

More recently, the "Zealandia-Antarctic" mantle domain has been designated between the Indian and Pacific mantle domains, relating to the break-up of Gondwana at ~90 Ma (Park et al., 2019). The Auckland volcanic field's $^3He/^4He$ signature of ~7 R_A is commonly observed throughout the Zealandia-Antarctic domain (Fig. 8; e.g. Hoke et al., 2000; Nardini et al., 2009; Day et al., 2019), and is similar to $^3He/^4He$ ratios along the Pacific-Antarctic Ridge (Moreira et al., 2008), parts of south-west Indian Ridge (SWIR) and in the 180 Ma Karoo flood basalt province (Georgen et al., 2003; Heinonen and Kurz, 2015). This low $^3He/^4He$ (~7 Ra) feature seems to stretch far beyond the region affected by the 90 Ma breakup of Gondwana, despite there being no obvious single mechanism linking the $^3He/^4He$ in these regions. Although extremely speculative, one possible explanation might be that large mantle plume events at ~180 Ma and ~90 Ma led to widespread dispersion of material in the upper mantle that today has $^3He/^4He$ near 7 Ra.

The homogeneity of the $^3He/^4He$ signature of the AVF compared to other isotopic and geochemical tracers (e.g. Pb isotopes and La/Yb, K/La, Ba/Rb ratios; McGee et al., 2013) raises the broader questions about possible "decoupling" of He isotopes. The preservation of isotopic heterogeneity in the mantle depends largely on the size of the heterogeneities, their rheological properties, and the time-scales of convective folding and mixing (Albarede, 2005). Preservation of Sr−Pb isotopic heterogeneity in the AVF (McGee et al., 2013, 2015), even within individual volcanic eruptions (McGee et al., 2015), implies a mantle mixing scenario similar to the S-Y-S (small- young- solid state) model of mantle heterogeneity proposed by Zindler et al. (1979) to account for the Nd isotopic variability in Reykjanes Peninsula basalts of Iceland. The S-Y-S scenario is more consistent with small-scale heterogeneities within a single mantle domain (sub continental lithospheric mantle) as opposed to a melting regime that involves both the asthenosphere and lithosphere. Prior work in the Auckland Volcanic Field established a correlation of basalt geochemistry with volcano size, degree of melting, and source enrichment (McGee et al., 2015). Possible decoupling of helium even for these small-scale features, might imply that small-scale heterogeneities embedded in the mantle dominate the helium budget during melting. Alternatively, relatively long homogenization times for helium may have allowed diffusive overprinting of the ambient mantle from the heterogeneities (Hart et al., 2008).

5. Conclusions

Olivine phenocrysts in lava and tephra from eight different volcanic centres, representing the isotopic diversity of basalts from the Auckland Volcanic Field, were analysed by crushing for $^3He/^4He$, and He and CO_2 concentrations. The CO_2/He ratio, and in particular the CO_2 abundance, vary inversely with indicators of trace element enrichment such as $La/Yb_{[N]}$. This implies that either the proposed carbonatized mantle source for the most trace element enriched alkali basalts actually contributes lesser amounts of carbon during melting than do other mantle components, or more likely, that early vapour saturation and gas loss efficiently removes carbon from the magmatic system prior to magma crystallization and the entrapment of melt in phenocrysts. Alternatively, the lower CO_2 abundance in smaller-degree partial melts might be explained by the trapping of different proportions of melt inclusions relative to fluid inclusions (CO_2-rich bubbles present in the magma at depth). The amount of CO_2 in melt inclusion shrinkage bubbles that is released by crushing phenocrysts may also vary with the rates of magma ascent and cooling following melt entrapment. The helium concentration, in contrast, does not vary with geochemical indicators of enrichment, possibly due to diffusive re-equilibration of trapped helium with the host melt during magma ascent, or to a predominance of helium trapped in fluid inclusions relative to melt inclusions. This implies that the CO_2/He ratio released during the crushing of olivine phenocrysts may be variably influenced by the magmatic history of crystallization, ascent, and cooling in addition to mantle source composition.

There are significant trace element and Pb-Nd-Sr isotopic variations in the AVF due to differences in the degree of melting of a heterogeneous mantle source, yet the $^3He/^4He$ ratio is remarkably uniform at

7.10 ± 0.26 R_A. AVF subalkaline basalts carry a slight indication of subduction-related metasomatism, but this process is not evident from the $^3He/^4He$ results. AVF xenocrystic olivine from the mantle lithosphere, as sampled at Lake Pupuke, has a lower $^3He/^4He$ ratio 6.47 ± 0.50 R_A. The uniformity of the He isotopic results in AVF olivine phenocrysts does not allow us to distinguish between a variably metasomatised mantle domain versus melting and mixing of multiple mantle domains (e.g. lithosphere and asthenosphere). The homogeneity of He isotope results appears to require either 1) a mantle helium budget dominated by small-scale heterogeneities, such that all partial melts carry the He isotope composition of the smaller heterogeneities, or 2) the occurrence of a widespread metasomatic event that led to $^3He/^4He$ homogenization across the mantle domain(s) such that all melts carry the same He isotope composition. Notably, AVF basalts resemble other mantle-derived magmas from the Zealandia-Antarctic mantle domain in their relatively narrow range of $^3He/^4He$ ratios (Patterson et al., 1994; Hoke et al., 2000; Nardini et al., 2009; Day et al., 2019).

Declaration of competing interest

The authors declare that they have no known competing financial interests or personal relationships that could have appeared to influence the work reported in this paper.

Acknowledgments

The helium isotope analyses at OSU were supported by the National Science Foundation through grants OCE15-58798 and 17-63255. Partial funding for Rowe was provided by University of Auckland Research and Study Leave support. The authors would also like to thank P. Wallace for access to his HFB_4 facility and L. Moore for discussions on volatiles in shrinkage bubbles. We thank Don Porcelli, James Scott and an anonymous reviewer for helpful comments on the manuscript.

References

Albarede, F., 2005. The survival of mantle geochemical heterogeneities. In: Van Der Hilst, R.D., Bass, J.D., Matas, J., Trampert, J. (Eds.), Earth's Deep Mantle: Structure, Composition, and Evolution. Geophysical Monograph Seriespp. 160. https://doi.org/10.1029/160GM04.

Brenna, M., Cronin, S.J., Smith, I.E.M., Tollan, P.M.E., Scott, J.M., Prior, D.J., Bambery, K., Ukstins, I.A., 2018. Olivine xenocryst diffusion reveals rapid monogentic basaltic magma ascent following complex storage at Pupuke Maar, Auckland Volcanic Field, New Zealand. Earth Planet. Sci. Lett. 499, 13–22.

Bucholz, C.E., Gaetani, G.A., Behn, M.D., Shimizu, N., 2013. Post-entrapment modification of volatiles and oxygen fugacity in olivine-hosted melt inclusions. Earth Planet. Sci. Lett. 374, 145–155.

Cook, C., Briggs, R.M., Smith, I.E.M., Maas, R., 2005. Petrology and geochemistry of intraplate basalts in the South Auckland Volcanic Field, New Zealand: evidence for two coeval magma suits from distinct sources. J. Petrol. 46, 473–503. https://doi.org/10.1093/petrology/egh084.

Coote, A., Shane, P., Fu, B., 2019. Olivine phenocryst origins and mantle magma sources for monogenetic basalt volcanoes in northern New Zealand from textural, geochemical and δ18O isotope data. Lithos 344-345, 232–246.

Dalton, H.B., Scott, J.M., Liu, J., Waight, T.E., Pearson, D.G., Brenna, M., Le Roux, P., Palin, J.M., 2017. Diffusion-zoned pyroxenes in an isotopically heterogeneous mantle lithosphere beneath the Dunedin Volcanic Group, New Zealand, and their implications for intraplate alkaline magma sources. Lithosphere 9 (3), 463–475.

Danyushevsky, L.V., McNeill, A.W., Sobolev, A.V., 2002. Experimental and petrological studies of melt inclusions in phenocrysts from mantle-derived magmas: an overview of techniques, advantages and complications. Chem. Geol. 183, 5–24.

Day, J.M.D., Harvey, R.P., Hilton, D.R., 2019. Melt-modified lithosphere beneath Ross Island and its role in the tectono-magmatic evolution of the West Antarctic Rift System. Chem. Geol. 518, 45–54.

Dixon, J.E., 1997. Degassing of alkali basalts. Am. Mineral. 82, 368–378.

Dunai, T., Porcelli, D., 2002. Storage and transport of noble gases in the subcontinental lithosphere. In: Porcelli, D., Wieler, R., Ballentine, C.J. (Eds.), Noble Gases in Geochemistry and Cosmochemistry. Mineral. Soc. Amer, Washington, D.C, pp. 371–409.

Finn, C.A., Muller, R.D., Panter, K.S., 2005. A Cenozoic diffuse alkaline magmatic province (DAMP) in the southwest Pacific without rift or plume origin. Geochem. Geophys. Geosyst. 6 (1). https://doi.org/10.1029/2004GC000723.

Gaetani, G.A., O'Leary, J.A., Shimizu, N., Bucholz, C.E., Newville, M., 2012. Rapid re-equilibration of water and oxygen fugacity in olivine-hosted melt inclusions. Geology 40, 915–918.

Gautheron, C., Moreira, M., 2002. He signature of the subcontinental lithospheric mantle. Earth Planet. Sci. Lett. 199, 39–47.

Gautheron, C., Moreira, M., Alegre, C., 2005. He, Ne and Ar composition of the European lithospheric mantle. Chem. Geol. 217, 97–112.

Georgen, J.E., Kurz, M.D., Dick, H.J.B., Lin, J., 2003. Low 3He/4He ratios in basalt glasses from the western Southwest Indian Ridge (10°–24°E). Earth Planet. Sci. Lett. 206, 509–528.

Graham, D.W., 2002. Noble gas isotope geochemistry of mid-ocean ridge and ocean island basalts: characterization of mantle source reservoirs. In: Porcelli, D., Ballentine, C.J., Wieler, R. (Eds.), Noble Gases in Geochemistry and Cosmochemistry. Reviews in Mineralogy and Geochemistry 47. pp. 274–318.

Graham, D.W., Humphris, S.E., Jenkins, W.J., Kurz, M.D., 1992. Helium isotope geochemistry of some volcanic rocks from Saint Helena. Earth Planet. Sci. Lett. 110, 121–131.

Graham, D.W., Hanan, B.B., Hémond, C., Blichert-Toft, J., Albarède, F., 2014. Helium isotopic textures in Earth's upper mantle. Geochem. Geophys. Geosyst. 15, 2048–2074.

Graham, D.W., Michael, P.J., Rubin, K.H., 2018. An investigation of mid-ocean ridge degassing using He, CO_2, and $\delta^{13}C$ variations during the 2005-06 eruption at 9°50'N on the East Pacific Rise. Earth Planet. Sci. Lett. 504, 84–93.

Haase, K.M., Renno, A.D., 2008. Variation of magma generation and mantle sources during continental rifting observed in Cenozoic lavas from the Eger Rift, Central Europe. Chem. Geol. 257, 192–202.

Hanan, B.B., Graham, D.W., 1996. Lead and helium isotope evidence from oceanic basalts from a common deep source of mantle plumes. Science 272 (5264), 991–995.

Hanyu, T., Kaneoka, I., 1997. The uniform and low 3He/4He ratios of HIMU basalts as evidence for their origin as recycled materials. Nature 390, 273–276.

Hanyu, T., Kawabata, H., Tatsumi, Y., Kimura, J.-I., Hyodo, H., Sato, K., Miyazaki, Chang, Q., Hirahara, Y., Takahashi, T., Senda, R., Nakai, S., 2014. Isotope evolution in the HIMU reservoir beneath St. Helena: implications for the mantle recycling of U and Th. Geochim. Cosmochim. Acta 143, 232–252.

Hart, S.R., Hauri, E.H., Oschmann, L.A., Whitehead, J.A., 1992. Mantle plumes and entrainment: isotopic evidence. Science 256 (5056), 517–520.

Hart, S.R., Kurz, M.D., Wang, Z., 2008. Scale length of mantle heterogeneities: constraints from helium diffusion. Earth Planet. Sci. Lett. 269, 507–516.

Hartley, M.E., Maclennan, J., Edmonds, M., Thordarson, T., 2014. Reconstructing the deep CO_2 degassing behaviour of large basaltic fissure eruptions. Earth Planet. Sci. Lett. 393, 120–131.

Heinonen, J.S., Kurz, M.D., 2015. Low-3He/4He sublithospheric mantle source for the most magnesian magmas of the Karoo large igneous province. Earth Planet. Sci. Lett. 426, 305–315.

Hilton, D.R., Fischer, T.P., Marty, B., 2002. Noble gases and volatile recycling at subduction zones. Rev. Mineral. Geochem. 47, 319–370.

Hodder, A.P.W., 1984. Late Cenozoic rift development and intra-plate volcanism in northern New Zealand inferred from geochemical discrimination diagrams. Tectonphysics 101, 293–318.

Hoernle, K., White, J.D.L., van den Bogaard, P., Hauff, F., Coombs, D.S., Werner, R., Timm, C., Garbe-Schonberg, D., Reay, A., Cooper, A.F., 2006. Cenozoic intraplate volcanism on New Zealand: upwelling induced by lithospheric removal. Earth Planet. Sci. Lett. 248, 350–367.

Hoke, L., Poreda, R., Reay, A., Weaver, S.D., 2000. The subcontinental mantle beneath southern New Zealand, characterised by helium isotopes in intraplate basalts and gas-rich springs. Geochim. Cosmochim. Acta 64 (14), 2489–2507.

Hopkins, J.L., Timm, C., Millet, M.-A., Poirier, A., Wilson, C.J.N., Leonard, G.S., 2016. Os isotopic constraints on crustal contamination in Auckland Volcanic Field basalts, New Zealand. Chem. Geol. 439, 83–97.

Horspool, N.A., Savage, M.K., Bannister, S., 2006. Implications for intraplate volcanism and back-arc deformation in northwestern New Zealand, from joint inversion of receiver functions and surface waves. Geophys. J. Int. 166, 1466–1483.

Horton, F., Farley, K., Jackson, M., 2019. Helium distributions in ocean island basalt olivines revealed by X-ray computed tomography and single-grain crushing experiments. Geochim. Cosmochim. Acta 244, 467–477.

Huang, Y., Hawkesworth, C., Smith, I., van Calsteren, P., Black, P., 2000. Geochemistry of late Cenozoic basaltic volcanism in Northland and Coromandel, New Zealand: implications or mantle enrichment processes. Chem. Geol. 164, 219–238.

Jiao, R., Seward, D., Little, A., Kohn, B.P., 2014. Thermal history and exhumation of basement rocks from Mesozoic to Cenozoic subduction cycles, central North Island, New Zealand. Tectonics 33, 1920–1935.

Johnson, D.M., Hooper, P.R., Conrey, R.M., 1999. XRF analysis of rocks and minerals for major and trace elements on a single low dilution Li-tetraborate fused bead. Adv. X-ray Anal. 41, 843–867.

Johnson, E.R., Wallace, P.J., Cashman, K.V., Granados, H.D., Kent, A.J.R., 2008. Magmatic volatile contents and degassing-induced crystallization at Volcan Jorullo, Mexico: Implications for melt evolution and the plumbing systems of monogenetic volcanoes. Earth Planet. Sci. Lett. 269, 478–487.

Knaack, C., Cornelius, S.B., Hooper, P.R., 1994. Trace Element Analyses of Rocks and Minerals by ICP-MS. Technical Notes, GeoAnalytical Lab. Washington State University.

Kokandakar, G.J., Ghodke, S.S., Rathna, K., More, L.B., Nagaraju, B., Bhosle, M.V., Kumar, K.V., 2018. Density, viscosity and velocity (ascent rate) of alkaline magmas. Journal Geological Society of India 91, 135–146.

Leonard, G.S., Calvert, A.T., Hopkins, J.L., Wilson, C.J.N., Smid, E.R., Lindsay, J.M., Campion, D.E., 2017. High-precision 40Ar/39Ar dating of Quaternary basalts from Auckland Volcanic Field, New Zealand, with implications for eruption rates and

paleomagnetic correlations. J. Volcanol. Geotherm. Res. 343, 60–74.
Matsuda, J., Maktsumoto, T., Sumino, H., Nagao, K., Yamamoto, J., Miura, Y., Kaneoka, I., Takahata, N., Sano, Y., 2002. The $^{3}He/^{4}He$ ratio of the new internal He Standard of Japan (HESJ). Geochem. J. 46, 191–195.
McCoy-West, A.J., Baker, J.A., Faure, K., Wysoczanski, R., 2010. Petrogenesis and origins of mid-Cretaceous continental intraplate volcanism in Marlborough, New Zealand: Implications for the long-lived HIMU magmatic mega-province of the SW Pacific. J. Petrol. 51 (10), 2003–2045.
McDonough, W.F., Sun, S.-s., 1995. The composition of the Earth. Chem. Geol. 120, 223–253.
McGee, L., 2012. Melting Processes in Small Volume Basaltic Systems: The Auckland Volcanic Field. University of Auckland, New Zealand PhD Thesis.
McGee, L., Smith, I.E.M., Millet, M.-A., Handley, H.K., Lindsay, J.M., 2013. Asthenospheric control of melting processes in a monogenetic basaltic system: a case study of the Auckland Volcanic Field, New Zealand. J. Petrol. 54 (10), 2125–2153.
McGee, L.E., Smith, I.E.M., 2016. Interpreting chemical compositions of small scale basaltic systems: a review. J. Volcanol. Geotherm. Res. 325, 45–60.
McGee, L.E., Millet, M.-A., Smith, I.E.M., Nemeth, K., Lindsay, J.M., 2012. The inception and progression of melting in a monogenetic eruption: Motukorea Volcano, the Auckland Volcanic Field, New Zealand. Lithos 155, 360–374.
McGee, L.E., Millet, M.-A., Beier, C., Smith, I.E.M., Lindsay, J.M., 2015. Mantle heterogeneity controls on small-volume basaltic volcanism. Geology 43 (6), 551–554.
Moore, L.R., Gazel, E., Tuohy, R., Lloyd, A.S., Esposito, R., Steele-MacInnis, M., Hauri, E.H., Wallace, P.J., Plank, T., Bodnar, R.J., 2015. Bubbles matter: assessment of the contribution of vapour bubbles to melt inclusion volatile budgets. Am. Mineral. 100, 806–823.
Moreira, M.A., Dosso, L., Ondreas, H., 2008. Helium isotopes on the Pacific-Antarctic ridge (52.5° - 41.4°S). Geophys. Res. Lett. 35, L10306. https://doi.org/10.1029/2008GL033286.
Mortimer, N., 2004. New Zealand's Geological Foundations. Gondwana Res. 7 (1), 261–272.
Nardini, I., Armienti, P., Rocchi, S., Dallai, L., Harrison, D., 2009. Sr-Nd-Pb-He-O isotope and geochemical constraints on the genesis of Cenozoic magmas from the West Antarctic Rift. J. Petrol. 50 (7), 1359–1375.
Nichols, A.R.L., Wysoczanski, R.J., Tani, K., Tamura, Y., Baker, J.A., Tasumi, Y., 2012. Melt inclusions reveal geochemical cross-arc variations and diversity within magma chambers feeding the Higashi-Izu Monogenetic Volcano Field, Izu Peninsula, Japan. Geochem. Geophys. Geosyst. 13 (9). https://doi.org/10.1029/2012GC004222.
Panter, K.S., Blusztajn, J., Hart, S.R., Kyle, P.R., Esser, R., McIntosh, W.C., 2006. The origin of HIMU in the SW Pacific: evidence from Intraplate Volcanism in the Southern New Zealand and Subantarctic Islands. J. Petrol. 47 (9), 1673–1704.
Park, S.-H., Langmuir, C.H., Sims, K.W.W., Blichert-Toft, J., Kim, S.S., Scott, S.R., Lin, J., Choi, H., Yang, Y.-S., Michael, P.J., 2019. An isotopically distinct Zealandia-Antarctic mantle domain in the Southern Ocean. Nat. Geosci. 12, 206–214.
Patterson, D.B., Honda, M., McDougall, I., 1994. Nobel gases in mafic phenocrysts and xenoliths from New Zealand. Geochim. Cosmochim. Acta 58 (20), 4411–4427.
Porcelli, D.R., O'Nions, R.K., Galer, S.J.G., Cohen, A.S., Mattey, D.P., 1992. Isotopic relationships of volatile and lithophile trace elements in continental ultramafic xenoliths. Contrib. Mineral. Petrol. 110, 528–538.
Poreda, R., Craig, H., 1989. Helium isotope ratios in circum-Pacific volcanic arcs. Nature 338, 473–478.
Rasoazanamparany, C., Widom, E., Valentine, G.A., Smith, E.I., Cortes, J.A., Kuentz, D., Johnsen, R., 2015. Origin of chemical and isotopic heterogeneity in a mafic, monogenetic volcanic field: a case study of the Lunar Crater Volcanic Field, Nevada. Chem. Geol. 397, 76–93.
Reid, M.R., Graham, D.W., 1996. Resolving lithospheric and sub-lithospheric contributions to helium isotope variations in basalts from the southwestern US. Earth Planet. Sci. Lett. 144, 213–222.
Reiners, P.W., 1998. Reactive melt transport in the mantle and geochemical signatures of mantle-derived magmas. J. Petrol. 39 (5), 1039–1061.
Roedder, E., 1979. Origin and significance of magmatic inclusions. Bull. Mineral. 102, 487–510.
Scott, J.M., Waight, T.E., van der Meer, Q.H.A., Palin, J.M., Cooper, A.F., Munker, C., 2014. Metasomatized ancient lithospheric mantle beneath the young Zealandia microcontinent and its role in HIMU-like intraplate magmatism. Geochem. Geophys. Geosyst. 15. https://doi.org/10.1002/2014GC005300.
Scott, J.M., Brenna, M., Crase, J.A., Waight, T.E., van der Meer, Q.H.A., Cooper, A.F., Palin, J.M., Le Roux, P., Munker, C., 2016. Peridotite lithosphere metasomatized by volatile-bearing melts, and its association with intraplate alkaline HIMU-like magmatisms. J. Petrol. 57, 2053–2078.
Seebeck, H., Nicol, A., Giba, M., Pettinga, J., Walsh, J., 2014. Geometry of the subducting Pacific plate since 20 Ma, Hikurangi margin, New Zealand. J. Geol. Soc. Lond. 171, 131–143.
Smith, I.E.M., Okado, T., Itaya, T., Black, P.M., 1993. Age relationships and tectonic implications of late Cenozoic basaltic volcanism in Northland, New Zealand. N. Z. J. Geol. Geophys. 36 (3), 385–393.
Sprung, P., Schuth, S., Munker, C., Hoke, L., 2007. Intraplate volcanism in New Zealand: the role of fossil plume material and variable lithospheric properties. Contrib. Mineral. Petr. 153, 669–687.
Stracke, A., Bourdon, B., 2009. The importance of melt extraction for tracing mantle heterogeneity. Geochim. Cosmochim. Acta 73, 218–238.
Strong, M., Wolff, J., 2003. Compositional variations within scoria cones. Geology 31, 143–146.
Sun, S.-s., McDonough, W.F., 1989. Chemical and isotopic systematics of oceanic basalts: implications for mantle composition and processes. Geological Society of London, Special Publications 42, 313–345.
Tucker, J.M., Mukhopadhyay, S., Gonnermann, H.M., 2018. Reconstructing mantle carbon and noble gas contents from degassed mid-ocean ridge basalts. Earth Planet. Sci. Lett. 496, 108–119.
Tucker, J.M., Hauri, E.H., Pietruszka, A.J., Garcia, M.O., Marske, J.P., Trusdell, F.A., 2019. A high carbon content of the Hawaiian mantle from olivine-hosted melt inclusions. Geochim. Cosmochim. Acta 254, 156–172.
Wallace, P.J., Kamenetsky, V.S., Cervantes, P., 2015. Melt inclusion CO_2 contents, pressure of olivine crystallization, and the problem of shrinkage bubbles. Am. Mineral. 100, 787–794.
Wang, S.-J., Teng, F.-Z., Scott, J.M., 2016. Tracing the origin of continental HIMU-like intraplate volcanism using magnesium isotope systematics. Geochim. Cosmochim. Acta 185, 78–87.
Woodhead, J.D., 1996. Extreme HIMU in an oceanic setting: the geochemistry of Mangaia Island (Polynesia), and temporal evolution of the Cook-Austral hotspot. J. Volcanol. Geotherm. Res. 72, 1–19.
Zindler, A., Hart, S.R., Frey, F.A., Jakobsson, S.P., 1979. Nd and Sr isotope ratios and rare earth element abundances in Reykjanes Peninsula basalts evidence for mantle heterogeneity beneath Iceland. Earth Planet. Sci. Lett. 45, 249–262.